Pergamon

Int. J. Heat Mass Transfer. Vol. 41, No. 17, pp. 2639–2652, 1998

Printed in Great Britain
0017–9310/98 $19.00+0.00

PII: S0017–9310(97)00324–4

Vortex interaction with a translating sphere in a stratified temperature field

M. MASOUDI† and W. A. SIRIGNANO
Department of Mechanical and Aerospace Engineering, University of California, Irvine, CA 92697, U.S.A.

(*Received* 24 *March* 1997 *and in final form* 8 *October* 1997)

Abstract—The three-dimensional interaction of an initially cylindrical vortex tube with a solid sphere in a stratified temperature field has been investigated by solving the Navier–Stokes and energy equations. Particular attention is given to the coupled effect on the sphere Nusselt number by the vortex advection and temperature stratification. Comparison with the sphere Nusselt number influenced by a vortex in a uniform temperature field [Masoudi and Sirignano, *Int. J. Heat Mass Transfer*, 1997, **40**(15), 3663–3673] shows that stratification has a profound effect on the sphere Nusselt number, qualitatively and quantitatively. Transient Nusselt number patterns are entirely different from those in a uniform temperature field; temperature stratification influences the vortex impact by nearly three fold. The sphere Nusselt number can be represented as the sum of Nusselt numbers in a uniform free-stream temperature at the average value and in a stratified stream with the given temperature variation and average temperature of zero. Therefore, in contrast to the commonly studied uniform free-stream case, stratification introduces an explicit dependence of the sphere Nusselt number on the temperature quantities. A correlation quantifying the coupled effect of the vortex-temperature stratification on the sphere heating, signifying a self-similar pattern in this unsteady problem has been produced. This correlation is also shown to be approximately valid for a liquid sphere. When the product of the vortex circulation and the gas-field temperature gradient is positive, the sphere time-averaged Nusselt number increases monotonically with an increase in the vortex circulation and with an increase in the vortex initial distance from the flow symmetry axis; when such product is negative, the Nusselt number increases with a decrease in vortex circulation or the vortex distance. Beyond a certain range of the vortex initial distance, the time-averaged Nusselt number reaches an asymptotic value. Based on these findings, it can be shown that in spray combustion systems coupled vortex-temperature stratification could have significant effect on droplets convective heating and their eventual evaporation.

1. INTRODUCTION

The fluid dynamics and heat transport for a cold liquid droplet in a hot gaseous axisymmetric environment are well-understood phenomena and there exists substantial literature exploring many different aspects of such problems [1]. There however is a shortage of literature exploring droplet heating and vaporization when the far-field flow embracing the droplet undergoes temporal and/or spatial variations in both the velocity and temperature fields. Existing literature has focused on variations due to acoustical waves [2, 3, 4]. The effect of vortical or thermal disturbances, as well as the effect of a coupling between the two, has not been widely examined.

There could exist two types of perturbations influencing the heating of a cold sphere in a hot gaseous environment-flow and thermal. Such a class of problems appears when the droplet transport properties are subject to velocity and temperature fluctuations in a turbulent flow, such as what might occur in a liquid-fueled combustor. In particular, in a combustor spray, the droplet size is ~ 100 microns. In the turbulence spectrum for many continuous combustors, this length-scale corresponds to that of the Kolmogorov scale; thus, the droplet transport phenomena can be subject to turbulent effects primarily associated with those of the Kolmogorov scale. Besides, droplets in a spray combustor are typically subject to, not a uniform but, a spatially varying temperature field in the gas phase (partly due to the 'stirring' effect of vortical structures and partly due to other parameters such as design constraints). Thus, the question remains to be one of coupled flow-thermal perturbations in the gas phase influencing droplet heating in combustors.

In this approach, we have considered turbulence as a manifestation of vortex dynamics [5]. We have represented the perturbation in the flow field by introducing an advecting Rankine vortex whose tangential velocity is weaker than the base flow. Furthermore, we have introduced an initially stratified temperature profile in the gas field to provide spatial variations in temperature. Thus, the coupled influence of the flow-thermal perturbations may be studied by introducing both an advecting vortex and an initially stratified temperature profile in the gas field.

Recent publications of the authors [6, 7] provided insight into the effect of hydrodynamic disturbances;

† Author to whom correspondence should be addressed.

NOMENCLATURE

a'	dimensional sphere radius (characteristic length)
d	vortex offset distance from the base flow symmetry axis (normalized by a')
Fo	Fourier number
N_1, N_2, N_3	number of grid points in (ξ, η, ζ)
Nu	Nusselt number
p	pressure
Pr	Prandtl number
q''	heat flux
r, θ, ϕ	spherical coordinates
Re	base flow Reynolds number (based on sphere diameter)
t	time (normalized by a'/U'_∞)
T	temperature
u, v, w	flow velocities in (x, y, z) directions (normalized by U'_∞)
v_{max}	maximum tangential velocity of vortex tube (normalized by U'_∞)
U'_∞	dimensional free stream velocity (characteristic velocity)
V	velocity vector
x, y, z	Cartesian coordinates.

Greek symbols

Γ	vortex tube circulation
κ	coefficient of initial temperature stratification
ν'	kinematic viscosity of the gas-phase
(ξ, η, ζ)	computational coordinates
σ	radius of vortex tube (normalized by a')
τ	shear stress
ψ	stream function
ω	vorticity.

Subscripts

ax	quantity in the corresponding axisymmetric flow (flow with no vortex)
g	quantity in the gas-phase
i	sphere surface (gas–solid interface)
mid	(middle) the grid point half-way between the first and the last one
s	quantity in the solid-phase
v	vortex quantity
0	initial quantity.

Superscript

$'$	dimensional quantity.

they introduced perturbations in the velocity field by introducing an advecting Rankine vortex. They reported new perspective into droplet heating influenced by vortical disturbances as well as a correlation signifying a self-similar behavior in such an unsteady problem [6]. The correlation compliments the existing ones for droplet heating in an axisymmetric flow [8].

In this work, we are extending the previous study by coupling the flow and thermal perturbations. Flow perturbations are again induced by an advecting vortex. Thermal perturbations are now represented by a spatially varying gas-phase temperature profile. In such a configuration, the vortex 'stirs' the flow and therefore mixes the relatively hotter gas with the colder gas near the sphere stimulating the convective heat transfer. Further description on the vortex structure and the gas-phase temperature profile are given in the sections Initial Conditions and Vortex Tube Features.

2. FLOW DESCRIPTION, GOVERNING EQUATIONS, AND VORTEX CHARACTERISTICS

Here, we present a summary of our approach covering the governing equations, the boundary and initial conditions, and the computational approach. Adequate references have been cited for further details.

Consider the three-dimensional, unsteady flow field surrounding a cold solid sphere impulsively injected in a hot gaseous environment with the sphere subsequently subjected to an unsteady interaction with a vortex tube. We numerically solve the governing equations for the velocity and the temperature fields; these are the Navier–Stokes and the thermal energy equations. The continuity equation is satisfied through pressure correction. The problem is nonlinear by nature. Constant properties are assumed in both the gas and the solid domain. The deceleration of the sphere due to the drag force is not considered. The equations and the boundary conditions are non-dimensionalized using the sphere radius a' as the characteristic length, the undisturbed free stream velocity U'_∞ as the characteristic velocity, and the average gas temperature far upstream $\bar{T}'_{g,\infty}$ as the characteristic temperature. The governing equations are:

Gas phase

$$\nabla \cdot V_g = 0 \tag{1}$$

$$\frac{DV_g}{Dt} = -\nabla p_g + \frac{2}{Re_g}\nabla^2 V_g \tag{2}$$

$$\frac{DT_g}{Dt} = \frac{2}{Re_g Pr_g}\nabla^2 T_g. \tag{3}$$

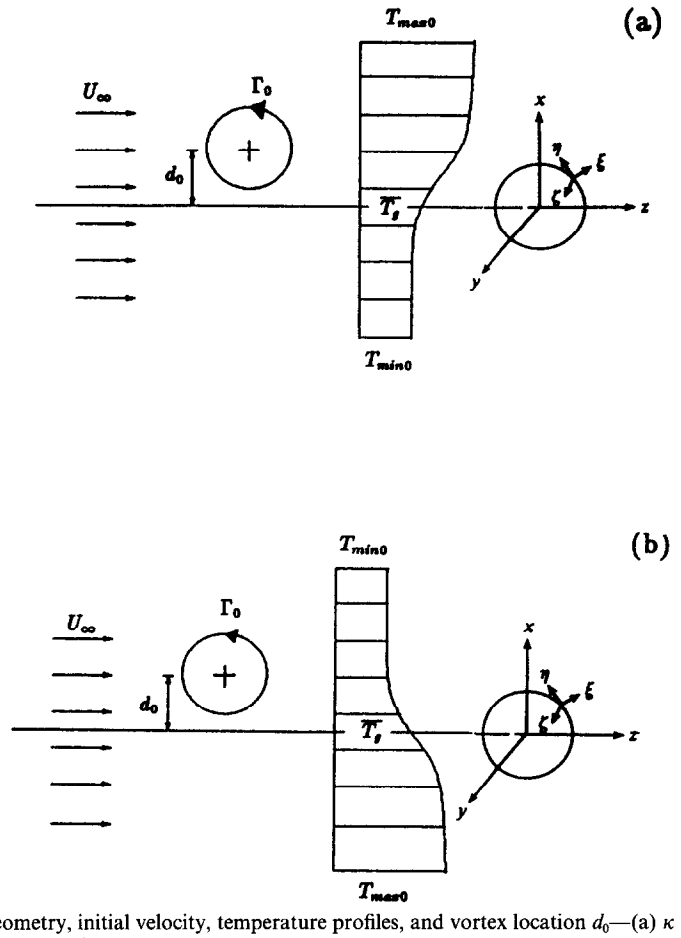

Fig. 1. Flow geometry, initial velocity, temperature profiles, and vortex location d_0—(a) $\kappa > 0$, (b) $\kappa < 0$.

Solid phase

$$\frac{\partial T_s}{\partial t} = \frac{2}{Fo}\nabla^2 T_s. \tag{4}$$

These governing equations are transformed to the coordinates (ξ, η, ζ); see Fig. 1. ξ is the radial, η is the angular, and ζ is the azimuthal direction. The numerical integration of the equations is performed using a computational cubic mesh with equal spacing $(\delta\xi = \delta\eta = \delta\zeta = 1)$.

2.1. *Gas–solid interface conditions*

The conditions at the interface are: zero normal, azimuthal, and polar velocity components, continuity of the heat flux and temperature. These conditions are conveniently cast in terms of spherical coordinates (r, θ, ϕ) with the origin at the center of the sphere. This allows the interface conditions to be applied at a constant value of the radius; also, the axisymmetric base case is more easily expressed. The (ξ, η, ζ) coordinates have the same orientation as the spherical coordinates (r, θ, ϕ) but obey an imposed stretching allowing a relatively denser grid concentration near the interface.

$$V_{g,r,i} = 0$$

$$V_{g,\theta,i} = 0$$

$$V_{g,\phi,i} = 0$$

$$T_{g,i} = T_{s,i}$$

$$q''_{g,i} = q''_{s,i}.$$

Here, q'' is the heat flux from the hot ambient gas into the cold sphere.

2.2. *Gas-phase boundary conditions*

(N_1, N_2, N_3) and (N_{1i}, N_2, N_3) are the number of grid points in the gas and solid domains, respectively, in (ξ, η, ζ) coordinates. ξ at N_{1i} and N_1 are the sphere surface and the gas farfield, respectively. The imposed far-field pressure, gas velocities in the x, y, z directions and gas temperature are

$$p = 0, \quad u = v = 0, \quad w = 1, \quad T = 1 \quad \text{at } \xi = N_1$$

and

$N_{2\text{mid}} \leqslant \eta \leqslant N_2$(upstream).

$$p = 0, \quad \frac{\partial u}{\partial \xi} = \frac{\partial v}{\partial \xi} = \frac{\partial w}{\partial \xi} = \frac{\partial T}{\partial \xi} = 0 \quad \text{at } \xi = N_1$$

and

$$1 \leqslant \eta < N_{2\text{mid}}(\text{downstream})$$

2.3. *Symmetry conditions*

Since the cylindrical vortex tube advects with its axis of symmetry parallel to the y-axis, symmetry is maintained with respect to the so-called principal plane—the y–z plane. We thus solve for half the spherical domain rather than the entire domain, and thus reduce the computational time.

$$\frac{\partial p}{\partial \zeta} = \frac{\partial u}{\partial \zeta} = \frac{\partial w}{\partial \zeta} = \frac{\partial T}{\partial \zeta} = 0; \quad v = 0 \quad \text{at } \zeta = 1, N_3.$$

Initial conditions

In the gas phase, the initial conditions for the velocity field are

$$u_0(x,y,z) = \frac{\Gamma_0}{\pi} \frac{z - z_{v0}}{[(x-x_{v0})^2 + (z-z_{v0})^2 + \sigma_0]^2}$$

$$v_0(x,y,z) = 0$$

$$w_0(x,y,z) = 1 - \frac{\Gamma_0}{\pi} \frac{x - x_{v0}}{[(x-x_{v0})^2 + (z-z_{v0})^2 + \sigma_0]^2} \quad (5)$$

i.e., the initial velocity in the gas phase is due to a uniform base flow ($u_0 = 0 = v_0, w_0 = 1$) and the cylindrical vortex ($\sim \Gamma_0$). In the absence of the vortex, the problem reduces to the well-studied axisymmetric flow around a sphere. Further description of the vortex is given in the section Vortex Tube Features.

The initial and free-stream gas-phase temperature, influencing the heat transfer to the sphere, is a crucial component of this study. We have imposed an initial and free-stream spatial temperature distribution of the form

$$T_0(x,y,z) = \left(\frac{T_{\max,0} + T_{\min,0}}{2}\right) + \left(\frac{T_{\max,0} - T_{\min,0}}{2}\right)\tanh(\kappa x) \quad (6)$$

which is shown in Fig. 1(a) and (b). The imposed temperature gradient has a length scale embodied in the coefficient κ^{-1}. The problem involves two other length scales—those of the flow (sphere radius) and the vortex. The coefficient κ, signifying the temperature gradient in the initially imposed stratified temperature profile, is chosen such that a physically realizable change in the temperature takes place over a length scale comparable to the sphere radius and the vortex length scale. If κ^{-1} is much smaller/larger than these other length scales, the effect of the stratification is too unrealistic/weak. We have chosen the values $0.15 \leqslant \kappa \leqslant 0.6$. This range of κ yields the change from $T_{\min,0}$ to $T_{\max,0}$ near the sphere over 15–3 length scales. Note equation (6) yields the average temperature $\bar{T}_g = (T_{\min,0} + T_{\max,0})/2$, the characteristic temperature, on the base flow symmetry axis. $\kappa > 0$ means that the initial gradient in the temperature profile aligns with the positive x-axis. We have considered temperature distributions with $\kappa > 0$ and $\kappa < 0$ for a full range of vortex initial positions.

Other possible profiles for the gas-phase initial temperature distribution, such as linear or exponential variations, were less interesting since they yield physically meaningless values for the temperature and so were not utilized. The hyperbolic tangent profile utilized appeared to yield a reasonable spatial change in the temperature.

The imposed initial solid sphere temperature is uniform with $T_{s,0} < T_{g,0}$. In the calculations, the sphere temperature was lower in value than the minimum free-stream fluid temperature; therefore, $T_{\min,0}$ is not the minimum temperature for the full flow field.

2.4. *Numerical solution*

A three-dimensional implicit finite-difference algorithm solves the set of discretized partial differential equations. The control volume formulation is used to develop the finite-difference equations. The method employs an Alternating-Direction-Predictor-Corrector (ADPC) scheme to solve the time-dependent equations.

The overall solution procedure is based on a cyclic series of estimate-and-correct operations. At each time-step, we first regard the solution in the gas-phase; the velocity components are first calculated from the momentum equations using the ADPC method, where the pressure field at the previous time step is employed. This estimate improves as the overall iteration continues. The pressure is calculated from the pressure correction equation using the successive over-relaxation method. The new estimates of pressure and velocities are then obtained. These known quantities are used in the energy equation to solve for the gas-phase temperature field.

Next, we use the interface conditions to solve for the interface values, followed by the sequential, iterative solution of the thermal energy equation in the solid-phase until convergence is achieved for each time step of the calculation.

At each time step, the drag, lift, and moment coefficients and Nusselt number of the sphere are evaluated. The entire procedure is then repeated for the next time-step. Further details may be found in previous publications of this research group [6, 7, 9, 10]. High precision computations for benchmarking purposes were executed on the Cray, taking an average runtime of about 5 cpu h. However, by using a normalization procedure (see end of the section The Sphere Convective Heat Transfer), we avoided such long computations and, using less mesh points, pursued most executions on a Dec-alpha or Convex 3840, taking average runtime of about 18 and 14 cpu min,

respectively, when $Re = 100$. Simulations for lower Reynolds number flows take longer to terminate executions since lower Reynolds number flow simulations require smaller time-steps; the time-step reduction (and thus the increase in the simulation time) is proportional to the reduction in Reynolds number. Analogous to our base computations, in this lower Reynolds number regime, the effect of change in our computational domain size on the result was also tested and negligible dependency between the two was observed.

2.5. *The vortex tube features*

The vortex is introduced upstream of the sphere, advects with the superimposed uniform flow, and has a relatively simple configuration—it is an initially cylindrical tube whose axis of symmetry is initially normal to the uniform flow and parallel to the y-axis. The vortex tube has a small central core; within this core, the initial velocity distribution in the vortex tube is that of solid body rotation reaching an imposed v_{max} at radius σ. v_{max} and σ are specified at time $t = 0$. Outside this inner core, the vortex induces a velocity field of a potential vortex; thus, the velocity induced by the vortex vanishes as $r \to \infty$. This two-dimensional vortical tube is known as a Rankine vortex [11], and has the following stream function [12]:

$$\psi_v(x, z, t = 0) = -\frac{\Gamma_0}{2\pi} \ln [(x - x_0)^2 + (z - z_0)^2 + \sigma_0^2] \tag{7}$$

where Γ_0 is the initial non-dimensional vortex circulation at radius σ_0. Γ_0 is positive when the vortex tube has counterclockwise rotation, and x_0 and z_0 denote the initial location of the center of the vortex tube. Note the initial vortex tube circulation at radius σ_0 is $\Gamma_0 = 2\pi\sigma_0 v_{max0}$. After the initial time, the advection, diffusion, and distortion (strain) on the vortex is determined through the solution of the Navier–Stokes equations. More fundamental information on the vortex tube such as temporal changes in its tangential velocity and vorticity are given in Ref. [7].

2.6. *Flow interaction*

The sphere is placed in a uniform flow (here also called the 'base flow') and thus, gradually develops a standing vortex ring in its aft position. Note that, in the absence of the vortex, the flow remains axisymmetric with respect to the z-axis (Fig. 1). The vortex is introduced 10 sphere radii upstream of the sphere and advects, initially, with the superimposed uniform free-stream flow and, later, with the local velocity; it takes about 10 residence time units for the vortex to arrive at the vicinity of the sphere; there, we observe vortex stretching in the cross-flow direction and thus, a full unsteady and three-dimensional interaction occurs between the vortex and the sphere. The dynamic interaction is the strongest when the vortex is initially introduced 'on' the base flow symmetry axis of Fig. 1; here, a 'head-on' collision between the sphere and the vortex is observed, resulting in a slowdown of the vortex advection and also vortex stretching in the cross-flow direction. When the vortex advects 'off' the axis, the dynamic interaction between the two is relatively weaker and the vortex therefore advects nearly steadily with the base flow. It takes nearly 25 residence time units for the vortex to arrive at the sphere, interact with it, and then travel sufficiently far downstream to have insignificant influence. Many details of the interactions were reported in Ref. [7].

2.7. *Flow and temperature perturbations*

There are five parameters that characterize the quantitative significance of the vortex–temperature stratification interaction with the sphere: the vortex initial core size (σ_0) and initial maximum tangential velocity (v_{max0}), the offset distance between the vortex initial position and the base flow symmetry axis (d_0), the base flow Reynolds number (Re), and the temperature gradient in the initial and free stream stratified temperature profile represented by κ [see equation (6), section on Initial Conditions]. We place the initial position of the vortex center either 'on' the base flow symmetry axis ($d_0 = 0$) or slightly 'off' it ($d_0 = \pm 1, \pm 2, \ldots$) and, as stated above, 10 sphere radii upstream of the sphere. A positive or negative d_0 means an offset distance from the z-axis in the x, z symmetry plane in the positive or negative x direction, respectively; this is shown in Fig. 1.

Reynolds number Re represents the base flow inertia—the underlying driving mechanism of the primary flow disturbed by the vortex-induced secondary flow. We specify an initial radius (σ_0) for the vortex which defines the vortex core within which vorticity is uniformly distributed; we select the strength of this vorticity so that the maximum velocity at the core of the vortex (v_{max0}) represents an acceptable fluctuation from the uniform flow. This fluctuation is taken to be less than the free stream velocity. For example, to represent a 20% fluctuation in the base flow, we pick $v_{max0} = 0.2$. Outside the inner core, the velocity pattern is that of a potential vortex. Thus, the vortex structure and strength are initially fully characterized by the two parameters σ_0 and v_{max0}, non-dimensionalized by the sphere radius and the strength of the uniform stream, respectively. The vortex initial circulation is $\Gamma_0 = 2\pi\sigma_0 v_{max0}$. Figure 1 shows a typical vortex location upstream of the sphere.

Γ_0, κ, and d_0 could each be either positive or negative. A positive Γ_0 is a counterclockwise vortex circulation; positive κ means the initial temperature gradient aligns with the positive x-axis in the principal x–z plane; a positive d_0 is an offset distance in the positive x-axis in the principal plane. We have studied all possible combinations of the signs of Γ_0, κ, and d_0 by keeping the vortex circulation counterclockwise and varying the signs of κ, and d_0. (Note that a simultaneous reversal of the sign of all three parameters

yields the same flow.) Our study covers $d_0 = 0, \pm 1, \pm 2, \pm 3, \pm 4, \pm 5$; $\sigma_0 = 0.25, 0.5, 1, 2, 3, 4$; $v_{max0} = 0.1, 0.2, 0.3, 0.4$; $20 \leqslant Re \leqslant 100$, and $0.15 \leqslant \kappa \leqslant 0.60$; this involves a range of vortex circulation varying by nearly two order-of-magnitudes: $\Gamma_0 \in (0.16, 10.05)$.

2.8. *Reduction of the computation cases*

The initial gas-field temperature profile is governed by equation (6). For particular values of Γ_0 and d_0, we need to compute the stratification effect for both positive and negative values of κ; this requires two computations. Furthermore, a different computation can be made for each set of maximum and minimum free stream temperature. Since the energy equation is linear in this constant-property simulation, it is instead possible, by using the superposition principle, to compute the sphere Nusselt number, first, for constant free stream and initial temperature

$$T_{(x,y,z)1} \equiv \frac{T_{max,0} + T_{min,0}}{2} \tag{8}$$

and, next, due to the temperature variation

$$T_{(x,y,z)2} \equiv \left(\frac{T_{max,0} - T_{min,0}}{2}\right) \tanh(\kappa x). \tag{9}$$

Summing the two results for the sphere Nusselt number yields the result for the Nusselt number in an initial temperature profile of the form

$$T_0(x,y,z) = T_{(x,y,z)1} + T_{(x,y,z)2} = \left(\frac{T_{max,0} + T_{min,0}}{2}\right) + \left(\frac{T_{max,0} - T_{min,0}}{2}\right) \tanh(\kappa x)$$

while subtracting them yields the Nusselt number due to

$$T_0(x,y,z) = T_{(x,y,z)1} - T_{(x,y,z)2} = \left(\frac{T_{max,0} + T_{min,0}}{2}\right) + \left(\frac{T_{max,0} - T_{min,0}}{2}\right) \tanh(-\kappa x).$$

The last two equations are the same as equation (6) with $\kappa > 0$ and $\kappa < 0$. Therefore, the Nusselt number with the sphere exposed to both possible orientations of the temperature gradient ($dT/dx \propto \kappa x, \kappa > 0, \kappa < 0$) are readily computed using superposition of the results. Furthermore, the Nusselt number for the stratified (second) portion will be proportional to the temperature term $(T_{max,0} - T_{min,0})/(T_{max,0} + T_{min,0})$; a scaling effect is obvious so that separate calculations for different values of $T_{max,0}$ and $T_{min,0}$ are not necessary.

A separate technique for reduction in computational time was also incorporated and has been discussed in the next section.

2.9. *The sphere convective heat transfer*

The sphere convective heat transfer, represented by its Nusselt number, is computed through $Nu(t) = 2a'h'/k'_g$ (with h' and k'_g being the convective heat transfer coefficient and the gas conductivity) which after a standard simplification and non-dimensionalization yields

$$Nu(t) = \frac{\int_0^{\pi}\int_0^{\pi} \left.\frac{\partial T_g(t)}{\partial r}\right|_s \sin\theta \, d\theta \, d\phi}{\pi(1 - \bar{T}_s)} \tag{10}$$

where $\bar{T}_s$ is the sphere temperature at the interface averaged over the surface.

Since the cold sphere is injected impulsively in the hot ambient gas, it initially experiences a stronger heat transfer and therefore a large Nusselt number. If the flow is axisymmetric and the gas temperature profile is uniform, the sphere Nusselt number gradually retains a steady value. In an axisymmetric flow, it takes nearly five resident time units for the sphere Nusselt number to reach a steady value. The flow pattern and therefore the Nusselt number is however different when a vortex advects in the base flow—the vortex advection breaks down the flow symmetry, Nusselt number fluctuates continuously and cannot attain a steady value. It is therefore more convenient to regard overall estimates by considering time-averaged and root-mean-squared values according to

$$\overline{Nu} = \frac{1}{t_2 - t_1} \int_{t_1}^{t_2} Nu(t) \, dt \tag{11}$$

and

$$Nu_{rms} = \sqrt{\overline{[Nu(t) - \overline{Nu}]^2}} = \sqrt{\frac{1}{t_2 - t_1} \int_{t_1}^{t_2} [Nu(t) - \overline{Nu}]^2 \, dt}. \tag{12}$$

Further, there is substantial computational advantage in normalizing $\overline{Nu}$ and Nu_{rms} using their corresponding values in an axisymmetric flow, $\overline{Nu}_{ax}$ and $Nu_{rms_{ax}}$. While different values are obtained for $\overline{Nu}$ depending on the number of computational mesh points (ordinarily, 41 in each direction), the same values of $\overline{Nu}/\overline{Nu}_{ax}$ are very well approximated with only half as many mesh points (21 in each direction) since both the numerator and denominator here change by the same amount, about 10%, due to reduction in mesh points. We therefore consider $\overline{Nu}/\overline{Nu}_{ax}$ and $Nu_{rms}/Nu_{rms_{ax}}$ in our results.

When the initial gas-phase temperature profile is uniform, Nu is a measure of the flow configuration due to the base flow and/or the vortex induced disturbances; i.e., it is independent of the characteristic temperature difference in the domain $(T' - T'_{s0})$. When the initial profile is stratified, and since $h' \sim q''/(\bar{T}' - T'_{s0})$ and $q'' \sim (T'_{max,0} - T'_{min,0})$, it results

that $Nu \sim (T'_{\max,0} - T'_{\min,0})/(\bar{T}' - T'_{s0})$. The non-dimensional form of the average free stream temperature $\bar{T}$ is given by equation (8). Therefore, the sphere Nusselt number is proportional to a non-dimensional temperature difference characterizing the initial conditions in temperature stratification and remains invariant to initial conditions in temperature for as long as this ratio is sustained. (Here, a high-order effect induced by the dependency of the thermophysical properties on temperature values is disregarded.) This noted difference with the uniform temperature case is of significance in understanding the sphere heat transfer in the stratified domain.

In equations (11) and (12), $t_1 = 2$ and $t_2 = 25$; i.e., we disregard the data for $t \in (0,2)$; this is the time needed for the initial computational fluctuations in the pressure drag to vanish. To minimize the influence of this initial data exclusion on the final outcome, we also estimate the normalizing values $\overline{Nu_{ax}}$ and $Nu_{rms_{ax}}$ with this criterion imposed. Computed $\overline{Nu}/\overline{Nu_{ax}}$ are more invariant to this initial data exclusion than $Nu_{rms}/Nu_{rms_{ax}}$. (Sample comparisons shown $\overline{Nu}/\overline{Nu_{ax}}$ and $Nu_{rms}/Nu_{rms_{ax}}$ values computed with and without this initial data exclusion vary by near or less than 0.05 and 8%, respectively.)

3. RESULTS

In the absence of the vortex, while the velocity field remains axisymmetric, the temperature stratification [equation (6)] yields an asymmetric temperature distribution; it also makes one side of the recirculation zone hotter than the other. The vortex advection breaks down the velocity field symmetry. The thermal boundary layer is affected by both the advection of the vortex and the temperature stratification. Also, the vortex could drastically change the structure of the recirculation zone in the sphere near wake and cause its otherwise confined pockets of vorticity to be ejected and to advect with the outer stream [7]. Further, due to the coupling between the velocity and temperature field, all developments in the velocity boundary layer induced by the vortex advection have their corresponding effect on the thermal boundary layer as well.

3.1. *Global self-similarity*

In the absence of the vortex, Nu and Nu_{ax} are identical; one may predict the sphere Nusselt number in an axisymmetric flow using the correlation [8]

$$Nu_{ax} = 1 + (1 + Pr\,Re)^{1/3}\, Re^{0.077} \quad Re \leqslant 400. \quad (13)$$

If a vortex advects in the gas-phase with an initially uniform temperature field and therefore perturbations are limited to that in the flow only ($\kappa = 0$, $\Gamma_0 \neq 0$), then the resulting deviations in Nusselt number due to the vortex are governed by [6]

$$\frac{\overline{Nu_{\kappa=0}}}{\overline{Nu_{ax}}} = 1 + 0.019 \frac{\Gamma_0}{2\pi} Re^{0.40} \tanh\left(0.50 \frac{d_0}{\sigma_0^{0.6}}\right) \quad (14)$$

so that $\overline{Nu_{\kappa=0}}/\overline{Nu_{ax}} - 1$ varies with change in vortex circulation Γ_0 and d_0 until $|d_0| \approx 2$ beyond which (but within $|d_0| \in [2,5]$) $\overline{Nu}/\overline{Nu_{ax}} - 1$ reaches an asymptotic value. This is shown in Fig. 2 and is well-discussed in ref. [6].

The situation is different when both flow and thermal perturbations coexist due to the simultaneous presence of the vortex and gas-phase temperature stratification. Here, the vortex 'stirs' the hotter gas with the cooler one near the sphere as well as itself inducting a secondary convective effect on the sphere heat transfer. Results for $Nu(t)$ in several representative cases are shown in Fig. 3(a) and (b). Consider, for instance, vortex advection with counter-clockwise circulation in a stratified temperature gas field with a positive temperature gradient ($dT/dx > 0, \kappa > 0$), and with the vortex advecting in the second quadrant of the principal x–z plane ($d_0 > 0$). With the vortex advecting upstream of the sphere, the cooler gas from the third and fourth quadrant (region of $T_{\min,0}$) is advected into the first and second and mixed with the hotter one (zone of $T_{\max,0}$), influencing $Nu(t)$ according to $Nu \sim q'' \sim (T'_{\max,0} - T'_{\min,0})$. Consequently, transient Nusselt number continuously fluctuates due to these combined effects of vortex-induced flow configuration and temperature variation.

Figure 4(a)–(c) show the temperature distribution near the sphere at various times. At earlier times, while the vortex is far upstream of the sphere and the velocity and thermal boundary layers are about to form, the domain is still relatively undisturbed (Fig. 4(a)). During this period, the sphere Nusselt number drops, as it does in an axisymmetric flow, to reach a steady value (Fig. 3(a) and (b), $t < 5$). Near $t \approx 10$, the thermal boundary layer is established, the vortex is near the sphere, the cooler and the hotter gas have been displaced due to vortex circulation (Fig. 4(a)) resulting in the fluctuation in Nusselt number (Fig. 3(a) and (b), $t \approx 10$). After the vortex advects downstream of the sphere, the recirculating effect of the vortex has an opposite effect resulting in a reversed fluctuation (Fig. 3(a) and (b), $10 < t < 20$). The fluctuation eventually vanishes as the vortex advects sufficiently downstream of the sphere (Fig. 4(c); Fig. 3(a) and (b), $t \to 25$).

Since the Nusselt number is a manifestation of the heat exchange between the gas and the sphere, it is not surprising that analogous fluctuations are observed for the sphere heat flux (Fig. 5).

Figure 6 shows a comparison for the transient Nusselt number influenced by vortex advection between the cases of a uniform and of a stratified temperature field. Previous observations [6] have shown that, in a uniform temperature field, when the vortex with positive circulation has an initial position upstream

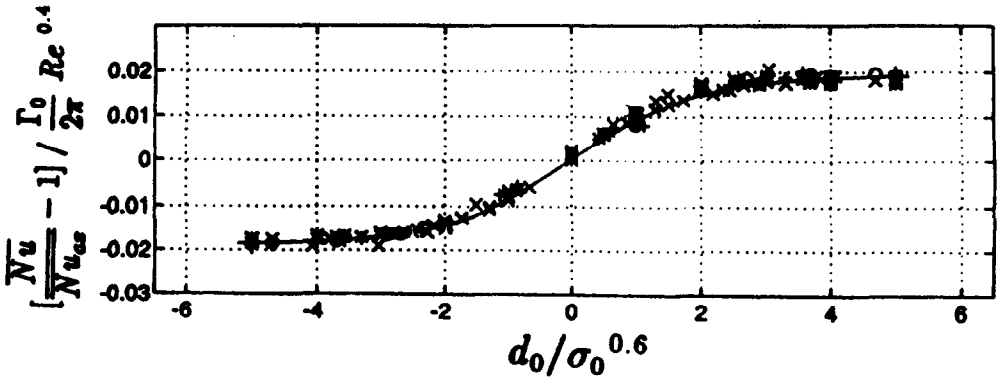

Fig. 2. Existence of self-similarity in time-averaged fluctuations of Nusselt number for a liquid or solid sphere influenced by vortex advection in a uniform temperature field [equation (14), from ref. [6]].

of the sphere and is 'above' the flow symmetry axis ($d_0 > 1$), $Nu(t)$ consistently 'overshoots' the axisymmetric pattern; the reverse is true when $d_0 < -1$; with $d_0 = 0$, $Nu(t)$ criss-crosses through the axisymmetric one. The stratification changes this picture qualitatively and quantitatively; vortex circulation transports the hotter gas to the cooler zone and vice versa and thus modifies substantially the sphere heat transfer; both the instantaneous and averaged heat transfer are modified.

The coupled vortical-stratification effect follow the correlations

$$\frac{\overline{Nu_{\kappa\neq 0}}}{\overline{Nu_{ax}}} = \frac{\overline{Nu_{\kappa=0}}}{\overline{Nu_{ax}}} + 2.04\left(\frac{T_{max,0}-T_{min,0}}{1-T_{s,0}}\right) \times \left(\frac{\Gamma_0}{2\pi}\right)^{1.1} \frac{\kappa^{0.8}}{d_0} \tanh\left(0.35\frac{d_0}{\sigma_0^{0.6}}\right); \quad \Gamma_0\kappa > 0 \quad (15a)$$

$$\frac{\overline{Nu_{\kappa\neq 0}}}{\overline{Nu_{ax}}} = \frac{\overline{Nu_{\kappa=0}}}{\overline{Nu_{ax}}} - 2.04\left(\frac{T_{max,0}-T_{min,0}}{1-T_{s,0}}\right) \quad (15b)$$

within the range of our parameter study: $20 \leqslant Re \leqslant 100$; $0.25 \leqslant \sigma_0 \leqslant 4$; $0.1 \leqslant v_{max0} \leqslant 0.4$; $-5 \leqslant d_0 \leqslant 5$, $0.15 \leqslant \kappa \leqslant 0.6$. This covers a range of vortex circulation varying by nearly two order-of-magnitudes: $\Gamma_0 \in (0.16, 10.05)$. All our simulations are for a solid sphere in hot air and so $Pr_g = 0.739$. Correlations (15) are shown in Fig. 7(a) and (b). The left-hand side of these equations represent the time-averaged value of the sphere Nusselt number while both flow and thermal perturbations are present. The first term on the right hand side (rhs) represents the sole vortex effect in a uniform temperature field, is from equation (14), and results as $\kappa \to 0$; the second term on the rhs is the coupled vortex-stratification effect. The second term on the rhs of equation (15a) or (15b) is an even function of d_0. Therefore, over our parameter range, the second term is always positive in equation (15a) and always negative in equation (15b). The linear summation of the two terms on the rhs is not surprising since the temperature satisfies a linear equation and superposition of the results is possible. Note that the uniform and the stratified temperature problems have identical velocity fields. The stratified free stream temperature can be viewed as the superposition of stratification, with positive and negative temperatures, onto a uniform temperature field at the average free stream temperature.

When κ is large, the regions of $T_{max,0}$ or $T_{min,0}$ temperatures are close to the sphere; by contrast, small κ means the regions at temperatures $T_{max,0}$ or $T_{min,0}$ are relatively far from the sphere. Qualitatively, in the former case, a small vortical perturbation 'stirs' the cooler and the hotter gas as much as a relatively large one does in the latter case. Thus, we expect that $\overline{Nu_{\kappa\neq 0}}/\overline{Nu_{ax}} - \overline{Nu_{\kappa=0}}/\overline{Nu_{ax}} \sim \Gamma_0^a \kappa^b$ where a and b are positive exponents. Furthermore, it is not surprising that, at large d_0, the perturbation decreases as d_0 increases. Similar behavior was observed in the uniform temperature study [6]. The overall effect is that $\overline{Nu_{\kappa\neq 0}}/\overline{Nu_{ax}} - \overline{Nu_{\kappa=0}}/\overline{Nu_{ax}} \sim \Gamma_0^a \kappa^b / d_0$ for large values of d_0, as shown by equations 15(a) and 15(b). [The exponents in equation (15) are chosen to reduce the data scattering and to optimize the fit.]

The first term on the rhs of equations (15) depends on both Re and Γ_0, and the second on Γ_0 only. This indicates that the stratification effect on the sphere Nusselt number, during vortex interaction, has the same Reynolds number dependence as the axisymmetric heat transfer case does. The Nusselt number for the sphere-vortex interaction in a uniform free stream temperature has a different Reynolds number dependence than the axisymmetric flow does [6], also seen by comparing equations (13) and (14).

In the absence of temperature stratification [equation (14)], the average sphere convective heat transfer may be augmented or reduced merely depending on the 'sign' of two parameters: the direction of the vortex-induced vorticity ($\Gamma_0 \sim \nabla \times \vec{v}_{max,0} = \vec{\omega}_0$ being

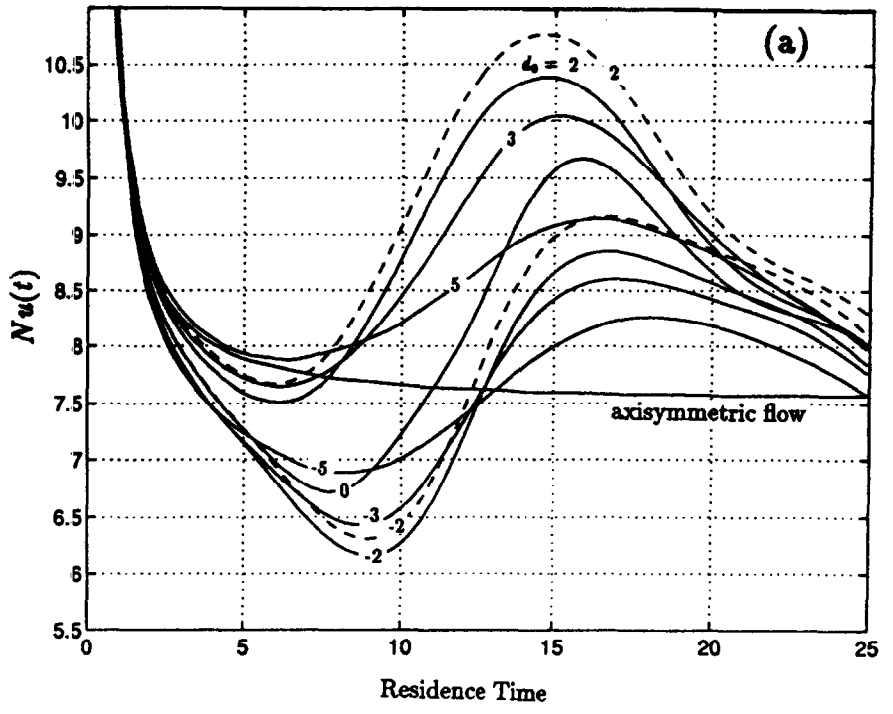

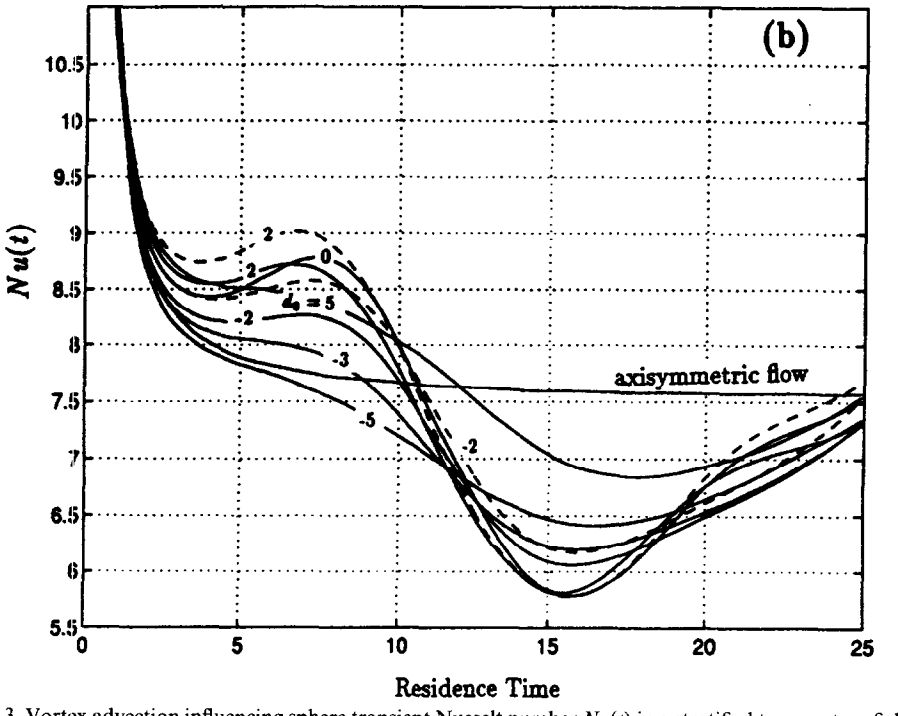

Fig. 3. Vortex advection influencing sphere transient Nusselt number $Nu(t)$ in a stratified temperature field, ($v_{max0} = 0.04$, $\sigma_0 = 1$, $Re = 100$) at various values of d_0; (a) $\kappa = 0.3 > 0$, (b) $\kappa = -0.3 < 0$. Dashed line is for a liquid sphere.

clockwise or counterclockwise) and the sign of the offset distance d_0; $d_0\Gamma_0 > 0$ augments the average sphere heat transfer while $d_0\Gamma_0 < 0$ reduces it. With the stratification present ($\kappa \neq 0$) where $\kappa > 0$ and $\kappa < 0$ refer to $dT_g/dx > 0$ and $dT_g/dx < 0$ in the free stream, respectively, equations (15) imply that counterclockwise circulation and positive temperature gradient ($\Gamma_0\kappa > 0$) augment the sphere Nusselt number. The Nusselt number is reduced when Γ_0 and κ have opposite signs. Equation (15) indicates that a change in the sign of either κ or circulation Γ_0 produces a change in the sign of the averaged Nusselt number deviation. A change only in the sign of d_0 produces a different $Nu(t)$ while, as seen in equations (15), $\overline{Nu}$ remains nearly unchanged.

Finally, we consider a cold liquid droplet in a hot gas subject to simultaneous perturbations both in the flow and temperature field, as is the case for droplets in a spray combustion system. Due to the large density ratio between the liquid and the gas phase, the liquid has a relatively higher inertia, keeping the droplet internal circulation weak. Thus, the droplet interface velocity remains very small compared to the free stream gas velocity. The dynamic viscosity of the liquid is significantly higher than the gas viscosity and also contributes to the reduction of the liquid velocity. However, the internal velocity is still an important factor in the droplet internal heat transfer. The structure of the viscous and thermal layers on the gas side of the interface do not change substantially, and so only minor changes in Nusselt number for the gas-phase boundary layer result. (However, internal circulation cannot be neglected because it will still have a significant effect on the interface temperature and, therefore, on the heat transfer through the gas-phase boundary layer.) These qualitative results are not changed by the thermocapillary effect at the interface [13, 14]. Therefore, we may approximate Nusselt number for a cold droplet (without vaporization) in a hot gas from correlations or simulations sought for a rigid sphere, and vice versa. We have further verified this in our investigation since simulations for a liquid sphere in the presence of an advecting vortex in a stratified temperature field yielded $\overline{Nu}_{\kappa\neq 0}/\overline{Nu}_{ax}$ values close to those for a solid sphere, fitting equations (15), and thus confirming that this correlation could be used for a liquid sphere in comparable condition, as well. This is also shown in Fig. 7.

Both correlations [equations (14) and (15)], consistent with the 'definition' of a perturbation, hold for bounded values of the fluctuating velocity; i.e., the vortex is not strong enough to reverse the free stream flow direction: $v'_{max0}/U'_\infty < 1$.

4. CONCLUSIONS

We have investigated the unsteady interaction between an initially cylindrical vortex tube and a solid sphere in a stratified temperature field, thereby allowing coupled flow-thermal perturbations to affect the sphere Nusselt number. Particular attention has been given to the transient and time-averaged values of Nusselt number. A correlation quantifying the simultaneous effect of the advecting vortex and temperature stratification on the sphere heating [equations (15)] has been produced, signifying a self-similar behavior for the average effect in this unsteady problem. The reported correlation compliments the existing correlations for a sphere heating in an axisymmetric flow without an advecting vortex [8], and also for a sphere heating perturbed solely by a vortical disturbance [6]. The correlation may also be used for a liquid sphere in comparable conditions in the presence of an advecting vortex.

Time-averaged Nusselt number is nearly linearly proportional to the vortex circulation and monotonically varies with change in the gas-phase temperature gradient; it also has a dependence on the vortex initial displacement from the sphere through the product of an algebraic and an exponential term; [see equations (15)]. Due to this exponential dependence, the influence of the vortex on the time-averaged Nusselt number reaches an asymptote for relatively larger d_0. Our computations here are limited to $|d_0| \leqslant 5$. Naturally, one expects that when the vortex advects 'very' far from the sphere, it will have negligible effect on the sphere heating; the correlations do not include the expected decay for equation (14) and for the first term on the rhs of equation (15).

Though this study concerned a particular setup of orientation and initial conditions for vortex advection and temperature stratification, and thus its findings are quantitatively limited to such particular couplings, the qualitative observations should have more general results. Namely, the coupled flow-thermal perturbations can have substantial effect on the heating mechanism, and the Nusselt number does not remain independent of the temperature values, an observation contrasting those in a uniform temperature field. Based on our findings, it may be speculated that, in a spray combustion system, the interaction between the naturally existing coupled flow-thermal perturbations and spray droplets within the Kolmogorov scale can have significant effects on droplet convective heat transfer and therefore on their eventual evaporation.

These calculations have not considered the effect of the deflection of the sphere due to the fluctuating velocity. Nor has the combined effects of an array of vortical structures been considered. These important issues should be addressed in the future.

Acknowledgements—The support of the University of California, Irvine, Office of Academic Computing through the use of their Convex C3840 and the help of Mr Donald Frederick and Dr Allen Schiano are gratefully appreciated. The San Diego Supercomputing Center also generously supported this work through their supercomputer time allocation.

Fig. 4. The thermal boundary layer of the sphere in the stratified temperature field influenced by the vortex advection; (a) $t = 2$; (b) $t = 10$; (c) $t = 25$; ($d_0 = 2$, $v_{max0} = 0.4$, $\sigma_0 = 1$, $\kappa = 0.3$, $Re = 100$).

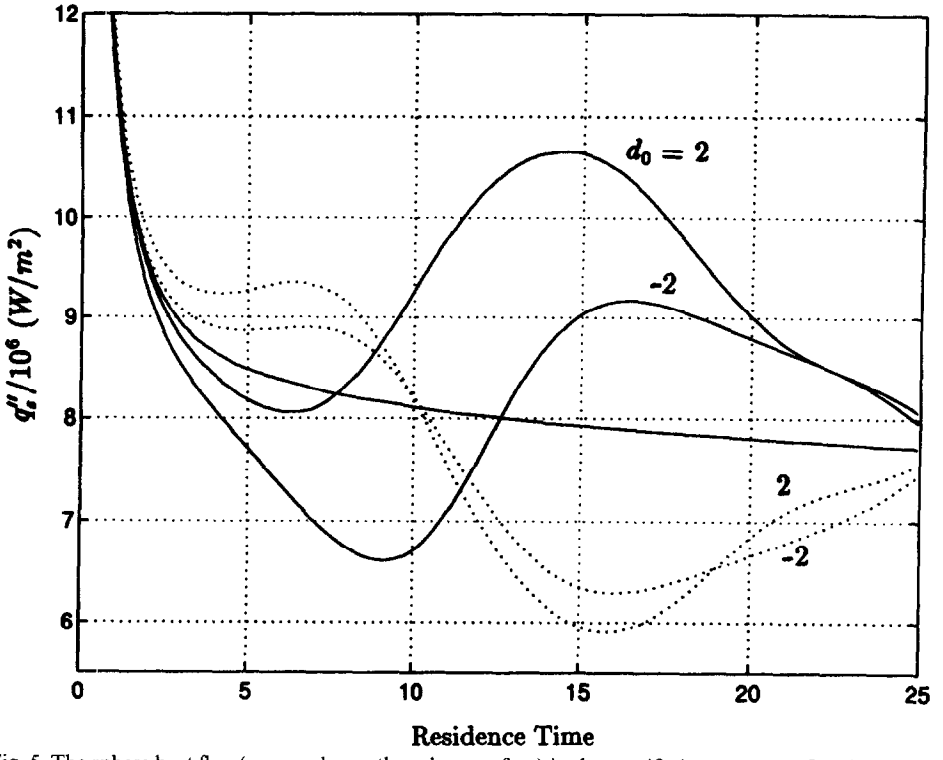

Fig. 5. The sphere heat flux (averaged over the sphere surface) in the stratified temperature field influenced by the vortex advection; ($v_{max0} = 0.4$, $\sigma_0 = 1$, $Re = 100$, $\kappa = +0.3$ solid line, $\kappa = -0.3$ dashed line).

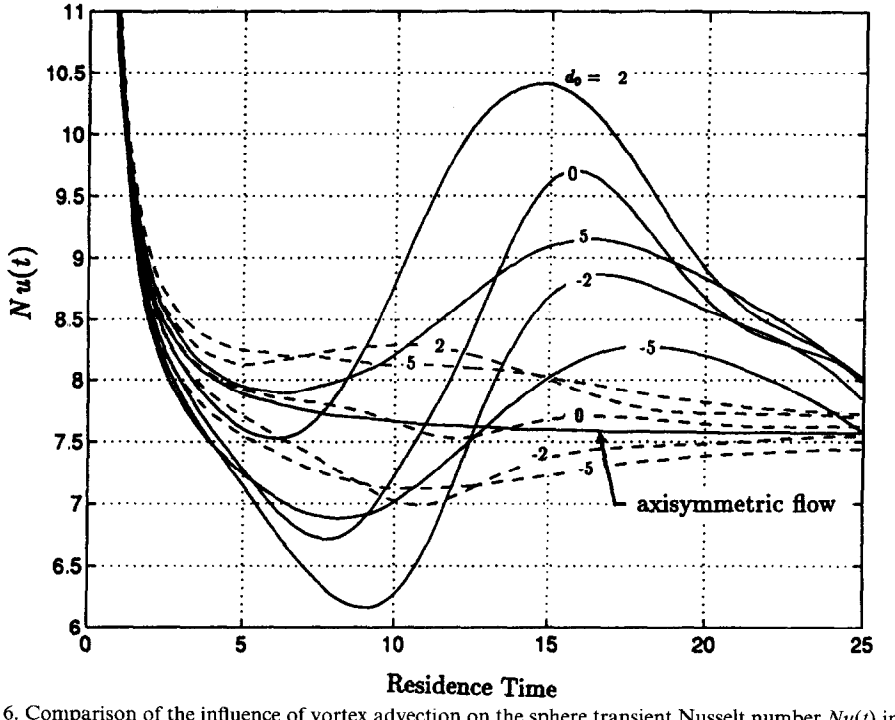

Fig. 6. Comparison of the influence of vortex advection on the sphere transient Nusselt number $Nu(t)$ in a uniform (dashed line) vs. a stratified (solid line) temperature field [$v_{max0} = 0.4$, $\sigma_0 = 1$, $Re = 100$, with $\kappa = 0$ (dashed line) and 0.3 (solid line)].

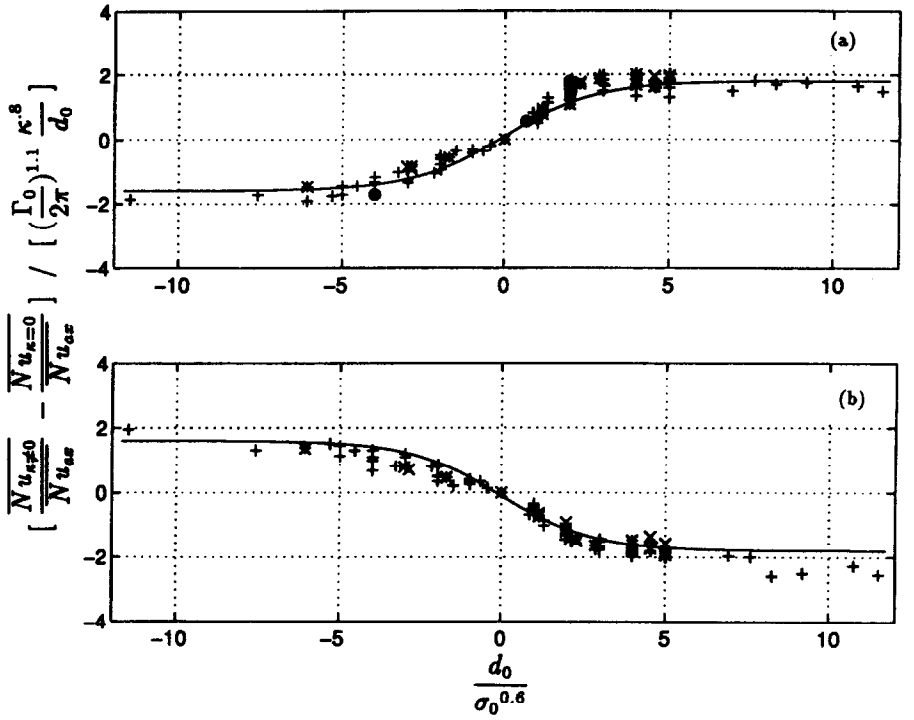

Fig. 7. Existence of self-similarity in time-averaged fluctuations of Nusselt number for a solid sphere influenced by vortex advection in a stratified temperature field [equation (15)], (a) $\kappa\Gamma_0 > 0$, (b) $\kappa\Gamma_0 < 0$. ● markers (at $d_0/\sigma_0^{0.6} = -4, 0.66, 1.98, 1.98$ each for $Re = 80, 100, 60, 100$, respectively) represent results of simulations for a liquid sphere.

REFERENCES

1. Sirignano, W. A., Fluid dynamics of sprays—1992 Freeman Scholar Lecture. *Journal of Fluids Engineering*, 1993, **115,** N3, 345–378.
2. Tong, A. Y. and Sirignano, W. A., Oscillating vaporization of fuel droplets in an unstable combustor. *Journal of Propulsion and Power*, 1989, **5,** 257–261.
3. Duvuur, A., Chiang, C. H. and Sirignano, W. A., Oscillating fuel droplet vaporization: driving mechanism for combustion instability. *Journal of Propulsion and Power*, 1996, **12,** N2, 358–365.
4. Abramzon, B. and Sirignano, W. A., Droplet vaporization model for spray combustion calculations. *International Journal of Heat and Mass Transfer*, 1989, **32,** 9, 1605–1618.
5. Chorin, A. J., *Vorticity and Turbulence*. Springer-Verlag, 1994.
6. Masoudi, M. and Sirignano, W. A., Influence of an advecting vortex on the heat transfer to a liquid droplet. *International Journal of Heat and Mass Transfer*, 1997, **40,** 15, 3663–3673.
7. Kim, I., Elghobashi, S. and Sirignano, W. A. Unsteady flow interactions between an advected cylindrical vortex tube and a spherical particle. *Journal of Fluid Mechanics*, 1995, **288,** 123–155.
8. Clift, R., Grace, J. R. and Weber, M. E., *Bubbles, Drops, and Particles*. Academic Press, 1978.
9. Kim, I., Elghobashi, S. and Sirignano, W. A., Unsteady flow interactions between a pair of advected vortex tubes and a rigid sphere. *International Journal of Multiphase Flow*, 1997, **23,** 1–23.
10. Kim, I., Elghobashi, S. and Sirignano, W. A., Three-dimensional flow over two spheres placed side by side. *Journal of Fluid Mechanics*, 1993, **246,** 465–488.
11. Saffman, P. G., *Vortex Dynamics*. Cambridge University Press, 1992.
12. Spalart, P. R., Numerical simulation of separated flows. Ph.D. dissertation, Stanford University, 1982.
13. Niazmand, H., Shaw, B. D., Dwyer, H. A. and Aharon, I., Effects of Marangoni Convection on Transient Droplet Evaporation. *Combustion Science and Tech.*, 1994, **103,** N1-6, 219–233.
14. Shih, A. T. and Megaridis, C. M., Thermocapillary flow effects on convective droplet evaporation. *International Journal of Heat and Mass Transfer*, 1996, **39,** 2, 247–257.